



Cite this: *J. Mater. Chem. C*, 2022, 10, 2562

Received 8th September 2021,
Accepted 1st November 2021

DOI: 10.1039/d1tc04257b

rsc.li/materials-c

Cocrystal engineering for constructing two-photon absorption materials by controllable intermolecular interactions†

Yihan Zhang,^{‡,a} Hongnan Wu,^{‡,a} Yuan Wang,^b Lingjie Sun,^{*,ac} Shuyu Li,^d Yiwen Ren,^a Yajing Sun,^a Fangxu Yang,^{*,a} Xiaotao Zhang^{ID,*,d} and Wenping Hu^{ac}

The design of two-photon absorption (TPA) materials based on cocrystal engineering is an emerging strategy for constructing nonlinear materials. Here we observe that a prepared BDBT-TCNB cocrystal can retain well the TPA properties from the donor BDBT molecules, but the TPA properties of a BDBT-OFN cocrystal are inhibited upon using the same donor molecule but changing the acceptor molecule of the cocrystal. *Via* comparing the crystal structures and spectral data of the two cocrystals, we find that BDBT-TCNB cocrystals have obvious intermolecular charge transfer interactions, while the BDBT-OFN cocrystals exhibit totally different intermolecular arene–perfluoroarene interactions. Moreover, strong charge transfer interactions involving the BDBT-TCNB cocrystal also promote an enhancement of the fluorescence intensity and an increase in the lifetime and photoluminescence quantum yield (PLQY) relative to the monomers. Therefore, this example proves that intermolecular interactions involving cocrystals can be controlled *via* carefully selecting the donor and acceptor molecules, and then the TPA properties of the cocrystals can be selectively adjusted, promoting the development of TPA materials prepared *via* cocrystal engineering.

Introduction

Much effort has been devoted to preparing novel nonlinear optical materials, which are important due to their fascinating and wide range of applications in the fields of non-destructive imaging of biological tissues,¹ photodynamic therapy,² three-dimensional (3D) optical data storage,^{3,4} up-converted lasing,⁵ *etc.* Two-photon absorption (TPA) materials, which exploit near-infrared excitation light (typically 700–1200 nm) to convert visible light with the advantages of high energy density, enhanced three-dimensional penetration depth and low fluorescence background, *etc.*, have attracted much attention.^{6–9} Thus, efficient material design strategies are urgently needed in this field. In recent years, some studies report that organic cocrystal engineering can serve as a new promising strategy for preparing new functional materials,^{10–12} wherein the synergistic and collective effects between different components make the materials exhibit novel and tunable optoelectronic properties, and it has broad application prospects in the fields of luminescence,^{13,14} organic field effect transistors,^{15,16} photo-response switches,^{17,18} and ferroelectric properties.¹⁹ In this context, organic cocrystal engineering for producing TPA materials relative to traditional synthesis methods provides an alternative and fresh way due to their noncovalent assembly with features of low cost, simple operation, and enhanced controllability of intermolecular interactions. For instance, a TPA cocrystal of 4-styrylpyridine and 1,2,4,5-tetracyanobenzene was prepared by selecting two TPA-free single components in our previous work, wherein the intermolecular charge transfer interactions between donor and acceptor molecules are responsible for the unexpected TPA property.²⁰ Stoddart and co-workers reported that the TPA properties could be retained by cocrystallization of two TPA monomers, and a near-infrared emissive characteristic coexists in the assembled cocrystals.²¹ However, investigations on achieving TPA materials by organic cocrystal engineering are still in their infancy, probably due to the TPA properties (*i.e.*, the near-infrared response wavelength, the emission wavelength in

^a Tianjin Key Laboratory of Molecular Optoelectronic Sciences, Department of Chemistry, School of Science, Tianjin University, Tianjin 300072, China.

E-mail: sunlingjie@tju.edu.cn, yangfangxu@tju.edu.cn

^b University of Chinese Academy of Science, Beijing 100049, China

^c Joint School of National University of Singapore and Tianjin University, International Campus of Tianjin University, Fuzhou 350207, China

^d Institute of Molecular Aggregation Science of Tianjin University, Tianjin 300072, China. E-mail: zhangxt@tju.edu.cn

† Electronic supplementary information (ESI) available: Crystallographic information from BDBT-TCNB and BDBT-OFN; spectral characterization and two-photon absorption characterization of the cocrystals; CIF files of BDBT-TCNB and BDBT-OFN. CCDC 2108048 and 2108051. For ESI and crystallographic data in CIF or other electronic format see DOI: 10.1039/d1tc04257b

‡ The authors contributed equally to this work.

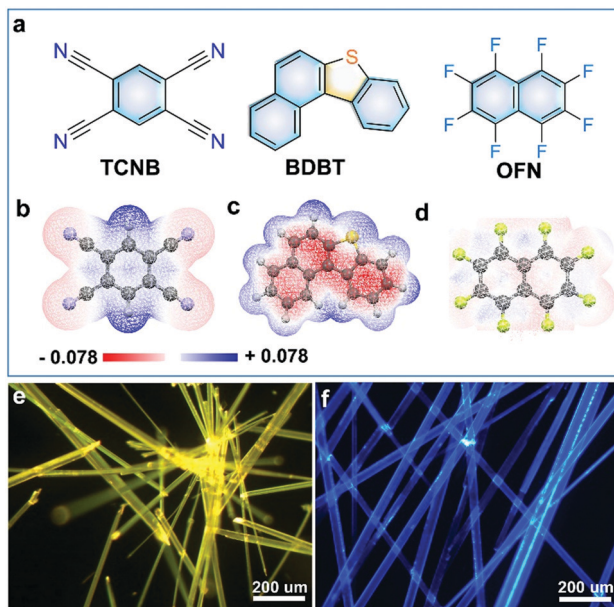


Fig. 1 (a) The molecular structures of TCNB, BDBT, and OFN. ESP maps of (b) TCNB, (c) BDBT, and (d) OFN. Fluorescence microscopy (FM) images of (e) BDBT-TCNB cocrystals and (f) BDBT-OFN cocrystals.

the visible region and two-phonon absorption cross-section) being affected by many factors, such as the size uniformity of the solid-state cocrystals, the molecular planarity of the donors and acceptors, and the degree of intermolecular charge transfer interactions between the donor and the acceptors. Thus, it is necessary to solve the problem of how to prepare a TPA material through cocrystal engineering. So how to choose the structural unit of the cocrystals and design the intermolecular interactions in cocrystals to control the properties of the cocrystals are very important and challenging.

Herein, we employed 1,2,4,5-tetracyanobenzene (TCNB) and octafluoronaphthalene (OFN) as electron acceptors, and benzo[*b*]naphtho[1,2-*d*]thiophene (BDBT) as an electron donor (Fig. 1a). Two new cocrystals with similar one-dimensional morphologies, called BDBT-TCNB and BDBT-OFN, were successfully designed and prepared by solution self-assembly methods. Although the same donor molecule of BDBT was used, the two cocrystals exhibited significantly different luminescence characteristics. Obvious yellow fluorescence for BDBT-TCNB with a red shift but blue fluorescence for BDBT-OFN with a blue shift relative to the BDBT molecules were observed. Through careful analysis of the cocrystal structure and spectral data of the two cocrystals, we found that the BDBT-TCNB cocrystals had obvious intermolecular charge transfer (CT) characteristics from donors to acceptors, while the BDBT-OFN cocrystals displayed arene-perfluoroarene (AP) interactions. Due to the strong charge transfer (CT) interactions in the BDBT-TCNB cocrystal system, BDBT-TCNB has unique and excellent properties, such as super-fluorescence intensity, long lifetime and PLQY. In addition, the monomer BDBT had good TPA properties, and the formed BDBT-TCNB cocrystals with CT interactions also retained TPA properties, and the two-

photon emission spectrum of the cocrystals was also red-shifted relative to the monomer. This showed that the cocrystal engineering with intermolecular charge transfer interactions could well inherit the TPA properties from the monomer. In contrast, the BDBT-OFN cocrystals with AP interactions had no TPA properties compared to the monomer, which may be caused by the longer distance of the light-emitting groups in the BDBT-OFN cocrystals than that of the BDBT. Collectively, the two cocrystals of BDBT-TCNB and BDBT-OFN exhibited different fluorescence emission characteristics with controlled intermolecular interactions relative to their monomers. Moreover, TPA properties were well preserved in BDBT-TCNB cocrystals and inhibited in BDBT-OFN cocrystals compared with their monomers, which provides a clear guideline for understanding cocrystal engineering strategies to construct TPA materials.

Results and discussion

In order to verify the molecular assembly ability between donors and acceptors, we calculated the surface electrostatic potential (ESP) of BDBT, OFN and TCNB. The blue areas and the red regions represent positive and negative potentials, respectively. As shown in Fig. 1c, the red area in the center of the BDBT molecule exhibits obvious electron-rich characteristics, indicating strong electron-donating behavior. The blue area on the benzene ring of the TCNB molecule exhibits an electron-deficient characteristic (Fig. 1b). The electron-attracting behavior is conducive to co-assembly with the BDBT molecule to form cocrystals with strong CT interaction. In contrast, OFN molecules exhibit a relatively even distribution of electrons, without strong electron-deficient and electron-rich characteristics, and may form other intermolecular forces with donor molecules. These results provide the possibility for the construction of cocrystals between different molecules. Subsequently, two cocrystals of compound BDBT with TCNB and OFN were obtained by a solvent slow volatilization method at room temperature. After the volatilization of the solution was completed, large crystals of millimeter-centimeter scale were obtained (Fig. S1, ESI[†]). In order to further study the growth orientation and intermolecular interaction of the cocrystals, micro-nano-sized cocrystals were prepared by the drop casting method. When the mixed BDBT-TCNB and BDBT-OFN (the molar ratio is 1:1) acetonitrile solution was dropped into glass substrates, respectively, both high-quality microwires could be grown after the evaporation of the solute (Fig. S3, ESI[†]). Fluorescence microscope (FM) images of BDBT-TCNB microwires (Fig. 1d) show that they emit uniform and intense yellow light compared to pure BDBT or TCNB (Fig. S2b and S2d, ESI[†]), which may be attributed to a typical CT transition between BDBT and TCNB.^{22,23} Surprisingly, the luminescence of the BDBT-OFN microwires is very similar to that of BDBT single donor molecules, both of which emit relatively weak blue light (Fig. 1f and Fig. S2b, ESI[†]). Therefore, we have successfully prepared two types of cocrystals, and different interactions may lead to their different luminescence properties.

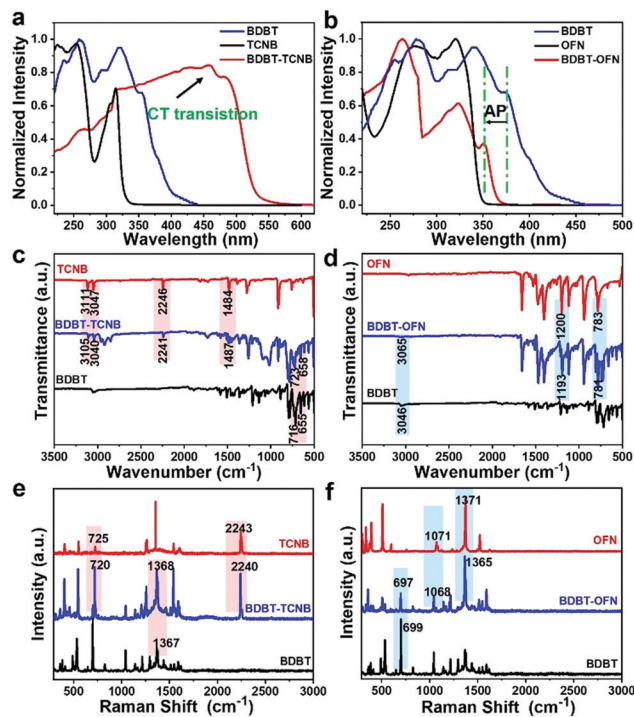


Fig. 2 The absorption spectra of (a) BDBT-TCNB cocrystals, (b) BDBT-OFN cocrystals, and the individual donor and acceptor materials. FTIR spectra of (c) BDBT-TCNB cocrystals, (d) BDBT-OFN cocrystals, and their respective constituent materials. Raman spectra of (e) BDBT-TCNB cocrystals, (f) BDBT-OFN cocrystals, and their respective constituent materials.

In order to explore the relationship between molecular interactions and photophysical properties, we conduct in-depth studies on the spectroscopy of solid-state crystalline samples. Obviously, absorption spectra can be used to distinguish intermolecular interactions. Compared with single-component BDBT crystals and TCNB crystals, BDBT-TCNB cocrystals exhibit a broader and significant red-shift in the absorption spectra (Fig. 2a), which indicates that there is a CT interaction from BDBT to TCNB in BDBT-TCNB cocrystals.²⁴ Interestingly, the absorption spectra of BDBT-OFN crystals show a clear blue shift compared with pure BDBT (Fig. 2b). The blue-shifted absorption is due to the electron-deficient electron barrier of OFN periodically inserted between adjacent BDBT molecules through $\pi \cdots \pi$ and C-F \cdots H interactions,^{25–27} which arises from the AP interactions between the BDBT and OFN molecules. The Fourier transform infrared (FTIR) spectrum and Raman spectrum of BDBT-TCNB are basically a combination of the BDBT and TCNB spectra (Fig. 2c and e). The sharp peak of BDBT-TCNB indicates that the cocrystal material is endowed with good crystal quality. The movement of peaks in BDBT-TCNB is caused by various intermolecular interactions. More importantly, the bands of TCNB show a slight movement after self-assembly into BDBT-TCNB cocrystals (C-H str: from 3111 cm^{-1} to 3105 cm^{-1} ; C≡N str: from 2246 cm^{-1} to 2241 cm^{-1} ; C=C str: from 1484 cm^{-1} to 1487 cm^{-1}), suggesting an increase in the electron cloud density on the benzene ring of TCNB (Fig. 2c).^{28,29}

Additionally, a few corresponding BDBT peaks in BDBT-TCNB also show a blue shift, revealing the CT interaction inside the molecule. From the Raman spectra, the 725 cm^{-1} of TCNB (ring bend) in BDBT-TCNB cocrystals is shifted to 720 cm^{-1} , indicating the increasing electron density.²⁰ In contrast, the peak position in the donor BDBT shifts to a high wavenumbers (Fig. 2e). Thus, the CT system is formed due to the readjusted charge distribution in the BDBT-TCNB cocrystals.³⁰ In the FTIR spectrum of BDBT-OFN,²⁷ the C-F bond in OFN shifts from 783 cm^{-1} to 781 cm^{-1} , and the C-F stretch signal moves from 1200 cm^{-1} to 1193 cm^{-1} (Fig. 2d). Such changes suggest that the C-F bond is weakened and lengthened because of the $n \rightarrow \sigma^*$ donation in BDBT-OFN cocrystals.²⁵ Additionally, the characteristic stretching peak of BDBT shifts from 3046 cm^{-1} to 3065 cm^{-1} , which is attributed to the C-F \cdots H interactions in the benzene ring.²⁶ The Raman spectrum of BDBT-OFN shows a small shift as well, which is ascribed to the internal molecular force derived from the AP interaction. In order to further prove the intermolecular interaction type of the two cocrystals, we adopted ultra-sensitive electron spin resonance (ESR) spectroscopy. The ESR spectrum of BDBT-TCNB displays a sharp signal with a g factor of 2.0032, indicating that there are unpaired electrons in the CT process of the ground state and the excited state (Fig. S8a, ESI[†]), while no signal was detected in BDBT-OFN (Fig. S8b, ESI[†]). From the above analyses, we can draw the conclusion that the intermolecular interactions of BDBT-TCNB and BDBT-OFN are CT interactions and AP interactions, respectively, which lays the foundation for us to explore the influence of intermolecular interactions on properties.

We further focused on the detailed structural information for BDBT-TCNB and BDBT-OFN to compare their stacking modes and effective intermolecular forces. Tested by single crystal diffraction, BDBT-TCNB is a triclinic crystal and belongs to the $P\bar{1}(2)$ space group with cell parameters of $a = 7.7920(3)\text{ \AA}$, $b = 8.0111(4)\text{ \AA}$, $c = 15.7519(9)\text{ \AA}$, $\alpha = 93.915(4)$, $\beta = 98.871(4)$ and $\gamma = 93.579(4)$ and $V = 966.59(8)\text{ \AA}^3$ (Table S1, ESI[†]). It is worth noting that the BDBT molecules in the BDBT-TCNB cocrystal are disordered, and the thiophene ring and the second benzene ring are equivalent. Therefore, the thiophene ring and the second benzene ring on the BDBT molecule each have a 50% occupancy rate. The donor and acceptor molecules in the BDBT-TCNB cocrystal show a mixed stacking mode. Among them, BDBT molecules and TCNB molecules are alternately arranged in a face-to-face pattern along the a -axis direction, and the distance between the D-A molecules along the π - π direction is 3.33 \AA , indicating that there is a strong D-A interaction in BDBT-TCNB.³¹ In addition, there are also N \cdots H-C and S \cdots H-C interactions between the molecules of the BDBT-TCNB cocrystals, which creates a pseudo-2D network in the (100) plane.³² So to gain a deeper understanding of the crystal structures, powder XRD measurements were analyzed. The BDBT-TCNB cocrystal shows different diffraction peaks from the single-component donor and acceptor. (All test powders were obtained by grinding large crystals made by a solution volatilization method.) In addition, the sharp diffraction peaks imply that BDBT-TCNB has a better crystal quality. And the analysis of the powder XRD results of the measured BDBT-TCNB

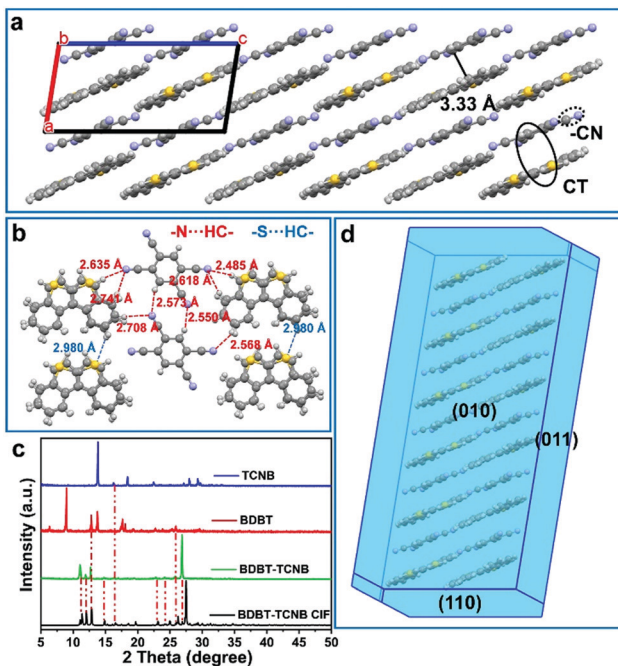


Fig. 3 The mixed-stack packing of BDBT-TCNB cocrystals. (b) Intermolecular interactions: N···H bonds and S···H bonds. (c) The powder X-ray diffraction (XRD) results of BDBT-TCNB, TCNB, and BDBT, and a calculated XRD pattern from the CIF file. (d) The predicted growth morphology of the BDBT-TCNB cocrystals.

is basically consistent with the simulation result of the CIF file (Fig. 3c), which also confirms the successful preparation of the cocrystals. Collectively, the BDBT-TCNB cocrystal prefers to fill the motif through face-to-face accumulation, which is driven by the charge transfer interactions. It is also conducive to the supramolecular electronic polarization in the cocrystals. Specifically, the formation of its pseudo-2D network makes it possible to enhance the two-photon absorption response.

Unlike the BDBT-TCNB crystal, BDBT-OFN is a monoclinic crystal and belongs to the $P 21/n$ space group with cell parameters of $a = 7.2054$ (2) Å, $b = 10.1966$ (3) Å, $c = 28.0448$ (7) Å, $\alpha = 90^\circ$, $\beta = 92.672$ (4) and $\gamma = 90^\circ$ and $V = 2058.23$ (10) Å³ (Table S1, ESI[†]). The distance between D and A along the π - π direction is 3.44 Å, and there are F···H-C interactions and S···H-C interactions between adjacent molecules (Fig. 4a). Therefore, a rigid 3D network is constructed through intra-column D-A interaction and multiple intra-column interactions (Fig. 4b). In powder XRD, the BDBT-OFN cocrystal shows the superposition of two monomer peaks, and some new diffraction peaks appear (Fig. 4c). Moreover, the sharp diffraction peaks imply that BDBT-OFN has a better crystal quality. In order to further understand and analyze the relationship between crystal structure and performance, Mercury software was used to calculate and analyze the intermolecular potential energy in the two types of cocrystal. Those results show that the face-to-face donor-acceptor interactions are the strongest intermolecular interactions in the cocrystal system. The intermolecular potential energy of BDBT-TCNB is -105.5 kJ mol⁻¹, and that of BDBT-OFN is -111.0 kJ mol⁻¹ (Fig. S7, ESI[†]). Therefore, the two types of cocrystals have different stacking structures

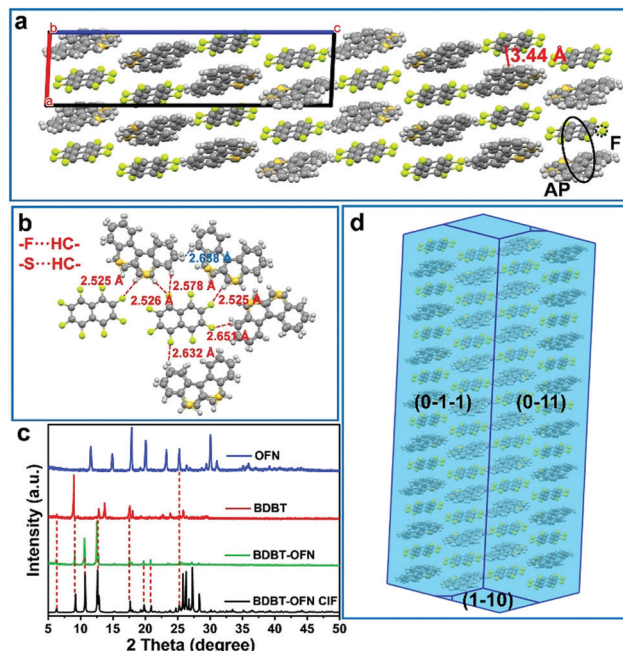


Fig. 4 (a) The mixed-stack packing of BDBT-OFN cocrystals. (b) Intermolecular interactions: S···H bonds and F···H bonds. (c) The powder X-ray diffraction (XRD) results for BDBT-OFN, OFN, and BDBT and a calculated XRD pattern from the CIF file. (d) The predicted growth morphology of the BDBT-OFN cocrystals.

and intermolecular forces, which is also the fundamental reason for the different photophysical properties.

The energy level diagram of the cocrystals and the monomer were depicted by simulation from density functional theory. The calculated energy diagrams (Fig. 5a) dictate that the HOMO of the BDBT-TCNB cocrystal is -6.13 eV that is related to the BDBT HOMO (-5.63 eV). And the electron cloud is mainly concentrated on the BDBT molecule. The LUMO (-3.36 eV) of BDBT-TCNB approaches the TCNB LUMO (-3.36 eV), and the electron cloud is also concentrated on TCNB. The apparent transfer in electron density is the result of CT interactions in the BDBT-TCNB cocrystal. In addition, BDBT-TCNB has a narrower band gap (2.77 eV), which is consistent with the red shift of the ultraviolet absorption spectrum. On the other hand, the HOMO of BDBT-OFN is -6.06 eV which is related to the BDBT HOMO (-5.63 eV), and the electron cloud is mainly concentrated on the BDBT molecule. However, the electron cloud of BDBT-OFN LUMO is evenly concentrated on the BDBT and OFN molecules with a high LUMO value of -1.60 eV. The band gap of the BDBT-OFN cocrystal becomes wider, which is consistent with its blue shift in absorption relative to the BDBT donors (Fig. 5b).

Photoluminescence (PL) spectroscopy was performed on two types of BDBT-based cocrystal to study the influence of different intermolecular forces on luminescence characteristics (Fig. 5c). The PL spectrum of the pure BDBT crystal shows the main emission peak near 390 nm. In contrast, BDBT-OFN shows a strong PL band at 376 nm, while BDBT-TCNB has only one band at 547 nm. Interestingly, compared with the PL

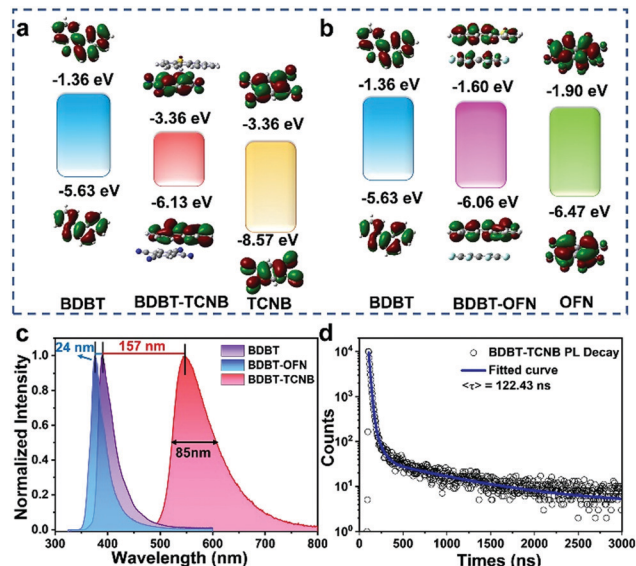


Fig. 5 (a) The calculated molecular orbital energy level diagrams of BDBT, BDBT-TCNB cocrystals, and TCNB. (b) The calculated molecular orbital energy level diagrams of BDBT, BDBT-OFN, and OFN. (c) PL spectra of BDBT-OFN, BDBT, and BDBT-TCNB. (d) The fluorescence decay curve of the BDBT-TCNB cocrystals.

spectrum of pure BDBT, the former has a blue shift of 14 nm, while the latter has a red shift of up to 157 nm. The BDTB-TCNB cocrystals display significantly red-shifted emission, due to the CT interactions between BDBT and TCNB after self-assembly. At the same time, the full width at half maximum (85 nm) of the BDBT-TCNB is also broadened and the Stokes shift has changed (Fig. S18, ESI[†]). The BDTB-TCNB cocrystals display significantly red-shifted emission, due to the CT interactions between BDBT and TCNB after self-assembly. At the same time, the full width at half maximum (85 nm) of the BDBT-TCNB is also broadened. The blue-shifted emission is attributable to the insertion of OFN molecules to shield the π interaction between two adjacent BDBT molecules, which significantly reduces the PL redshift caused by exciton delocalization.^{25,26} Besides, the fluorescence decay curve indicates that the PL lifetime of the BDBT-TCNB cocrystals is 122.43 ns with a three-exponential form (Fig. 5d). The fluorescence lifetime of the BDBT-TCNB cocrystal is significantly improved compared to the monomer (BDBT: 1.32 ns, TCNB: 4.83 ns, Fig. S10, ESI[†]), which is attributed to the stronger intermolecular interaction of the charge transfer cocrystal. It plays a key role in suppressing the rotation and vibrational non-relaxation of the excited state, thus extending the life of the cocrystal. At the same time, the photoluminescence quantum yield (PLQY) of the BDBT-TCNB crystal (11.44%) is also higher than that of the single component (BDBT: 3.04%; TCNB: 3.40%). Unlike previous reports, the incorporation of OFN did not improve the luminescence properties of BDBT materials. However, the fitting of the emission decay curve of BDBT-OFN is still in the form of three exponentials, and the fluorescence lifetime is estimated to be 1.18 ns. The lifetime of BDBT-OFN is shorter than that of single-component crystals (BDBT: 1.322 ns; OFN: 3.45 ns, Fig. S10, ESI[†]). Its PLQY is only 0.95%, which is

many times lower than those of the BDBT donor (3.04%) or OFN acceptor (4.21%). We speculate that the addition of OFN could cause fluorescence quenching. When an extensive amount of OFN solution is added into the BDBT solution, the fluorescence intensity is decreased greatly (Fig. S11, ESI[†]). The reason for the fluorescence quenching is that OFN molecules with weaker luminescence intensity are periodically inserted into the BDBT donor. The inserted OFN barrier separates two adjacent BDBT molecules and increases their distance from 3.454 Å to 6.749 Å (Fig. S13, ESI[†]). Because there is only a relatively weak AP interaction, the overall effect of BDBT is “diluted”, resulting in weaker luminescence. The luminescence color of BDBT-TCNB and BDBT-OFN cocrystals is obviously different from that of single-component crystals. The difference in luminescence can be seen from the CIE coordinates (Fig. S12, ESI[†]). In brief, the preparation of materials with tunable wavelength is realized by means of cocrystallization. The enhanced PLQY value of the BDBT-TCNB cocrystal allows the TPA phenomenon to be observed.

Given that the intermolecular interactions can have an effect on the cocrystal properties, the two-photon absorption characteristics (TPA) of the two cocrystals were studied. Two-photon absorption is a nonlinear optical process, which can take place when samples are irradiated by a high-intensity laser. Two-photon absorption characteristics exist in the BDBT donor and BDBT-TCNB cocrystal. Under the excitation of 700 nm and 800 nm lasers, the images of BDBT and BDBT-TCNB were observed through a two-photon microscope (Fig. S14 and S15, ESI[†]). The emission of the BDBT donor is collected in the blue detection channel, which closely corresponds to the position of its fluorescence emission (390 nm). In the same way, the emission of the BDBT-TCNB cocrystal is collected in the red detection channel. As the laser power density increases, the fluorescence intensity of the BDBT donor and the BDBT-TCNB cocrystal is square correlated with the incident energy (Fig. 6a and b), which means that the up-conversion emission originates from the two-photon absorption process. Fig. 6d reveals the TPA process in BDBT and BDBT-TCNB. A single photon excites the molecule to reach a virtual intermediate state, and takes the molecule to an excited state by absorbing the second photon in a short time.³³ The BDBT molecule exhibits TPA characteristics in the solid state, which may be due to the strong π - π interaction between the herringbone stacks to promote the π overlap within the molecule. The excellent TPA performance of BDBT-TCNB is due to the delocalization of π electrons caused by charge transfer within the molecules, thereby resulting in supramolecular electronic polarization in the cocrystal.³⁴ As expected, the BDBT-OFN cocrystal does not exhibit TPA characteristics. The reason is that the incorporation of OFN disrupts the electron delocalization of donor molecules, resulting in weaker electronic communication between molecules. In general, by controlling the intermolecular interaction of the cocrystal, we successfully realized the controllable adjustment of the emission wavelength and performance of the cocrystal. This also proves that ideal functionalized materials can be prepared by means of cocrystallization.

The thermal stability of the cocrystals and single components was studied. The thermogravimetric analysis (TGA) curve shows

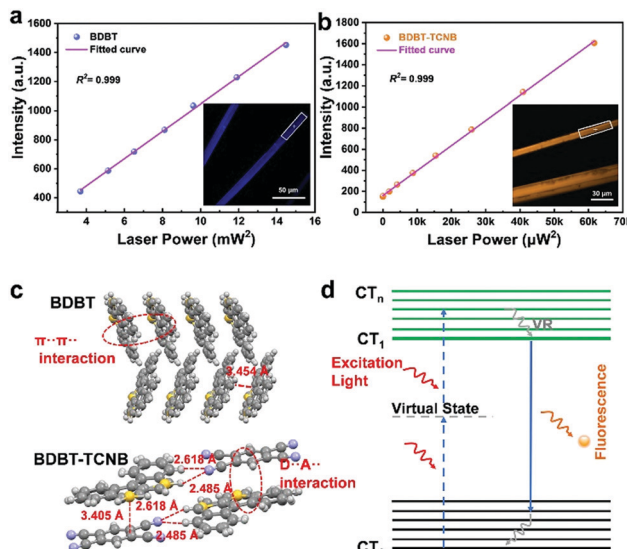


Fig. 6 The relationship between the fluorescence intensity and the square of the laser power for (a) a micron-wire of BDBT excited at 700 nm and (b) a micron-wire of BDBT-TCNB excited at 800 nm; the insets show two-photon microscope images of BDBT and BDBT-TCNB. (c) Molecular interaction forces of BDBT donors and BDBT-TCNB cocrystals. (d) A schematic diagram of the two-photon transition relating to BDBT and BDBT-TCNB.

that the sublimation points of BD, TCNB and BDBT-TCNB are 207 °C, 234 °C and 223 °C, respectively (Fig. S17a, ESI[†]). The sublimation point of the BDBT-TCNB cocrystal is different from that of the single component, indicating the formation of a new crystal lattice. However, the TGA curve of BDBT-OFN shows two typical gradient forms. And the corresponding sublimation temperatures of OFN and BDBT in the cocrystal are 138 °C and 212 °C, respectively (Fig. S17b, ESI[†]). When the temperature reached 185 °C, the OFN molecules completely disappeared. At this time, BDBT-OFN contributes 46.3% of the incipient weight, which is practically consistent with the actual weighted mass ratio of the acceptor and the donor in the cocrystal.³⁵ The high melting point and high sublimation point indicate the stable structure of BDBT-TCNB and BDBT-OFN. In addition, the melting points of the donor, acceptor and cocrystals are analyzed with a differential scanning calorimetry (DSC) diagram. Evidently, the melting point of BDBT-TCNB is 249 °C, which is different from those of individual BDBT crystals or TCNB crystals (Fig. S16a, ESI[†]).^{36,37} The result of the higher melting point figures is that the cocrystal has good thermostability because of the strong intermolecular interaction. The melting points of BDBT-OFN, BDBT and OFN are 98 °C, 104 °C and 88 °C, respectively, which means that the cocrystal has a new crystal lattice (Fig. S16b, ESI[†]). The above all indicate that the cocrystals are endowed with better thermal stability, which is convenient for future applications.

Conclusions

In summary, we have successfully prepared two kinds of cocrystals (BDBT-TCNB and BDBT-OFN) with good thermal stability *via* a solution self-assembly method. The intermolecular

interactions of these two cocrystals have been studied in depth based on clear cocrystal structures and spectral characterization. In detail, the BDBT-TCNB cocrystals exhibit intermolecular charge transfer characteristics, facilitating the spatial delocalization of free electrons, thereby allowing them to inherit the TPA properties of the BDBT molecules. BDBT-TCNB shows excellent optical properties, and the modification of materials provides new ideas. However, the BDBT-OFN cocrystals exhibit totally different arene-perfluoroarene interactions, in which OFN molecules block the delocalization of free electrons between donor molecules, thereby inhibiting the TPA performance of the cocrystals. Therefore, cocrystal engineering can realize the controllable appearance of TPA properties *via* selecting appropriate building blocks, providing new ideas for the preparation and application of TPA materials.

Author contributions

Lingjie Sun, Fangxu Yang, Xiaotao Zhang, and Wenping Hu conceived and supervised this study; Yihan Zhang and Hongnan Wu performed the material preparation and characterization; Yuan Wang assisted in characterizing the two-photon performance of the material; Yihan Zhang, Hongnan Wu, Shuyu Li, Yiwen Ren, and Lingjie Sun wrote the paper; Yajing Sun performed theoretical calculations. All authors contributed to discussions and manuscript review.

Conflicts of interest

There are no conflicts of interest to declare.

Acknowledgements

This work was supported by the National Key R&D Program (2017YFA0204503), the National Natural Science Foundation of China (91833306, 51903186, 21875158, 51633006, 51733004), and the China Postdoctoral Science Foundation (2019T120183, 2021M692381).

Notes and references

- 1 M. K. Kim, C. S. Lim, J. T. Hong, J. H. Han, H.-Y. Jang, H. M. Kim and B. R. Cho, *Angew. Chem., Int. Ed.*, 2010, **49**, 364–367.
- 2 X. Q. Shen, L. Li, A. C. M. Chan, N. Y. Gao, S. Q. Yao and Q. H. Xu, *Adv. Opt. Mater.*, 2013, **1**, 92–99.
- 3 C. O. Yanez, C. D. Andrade, S. Yao, G. Luchita, M. V. Bondar and K. D. Belfield, *ACS Appl. Mater. Interfaces*, 2009, **1**, 2219–2229.
- 4 B. H. Cumpston, S. P. Ananthavel, S. Barlow, D. L. Dyer, J. E. Ehrlich, L. L. Erskine, A. A. Heikal, S. M. Kuebler, I. Y. S. Lee, D. McCord-Maughon, J. Q. Qin, H. Rockel, M. Rumi, X. L. Wu, S. R. Marder and J. W. Perry, *Nature*, 1999, **398**, 51–54.
- 5 F. Todisco, I. Fortunati, S. Gardin, E. Garbin, E. Collini, R. Bozio, J. J. Jasieniak, G. Della Giustina, G. Brusatin,

S. Toffanin and R. Signorini, *Adv. Funct. Mater.*, 2012, **22**, 337–344.

6 X. Liang, W. J. Lin, B. B. Huang, J. Z. Zhang, X. T. Long, W. Y. Zhang and Q. C. Zhang, *J. Mater. Chem. C*, 2021, **9**, 1520–1536.

7 J. L. Humphrey and D. Kuciauskas, *J. Am. Chem. Soc.*, 2006, **128**, 3902–3903.

8 E. Garoni, J. Zirzlmeier, B. S. Basel, C. Hetzer, K. Kamada, D. M. Guldi and R. R. Tykwiński, *J. Am. Chem. Soc.*, 2017, **139**, 14017–14020.

9 Z. S. Gan, Y. Y. Cao, R. A. Evans and M. Gu, *Nat. Commun.*, 2013, **4**, 2061.

10 Y. Wang, J. Yang, Y. Gong, M. Fang, Z. Li and B. Z. Tang, *Smart Mater.*, 2020, **1**, e1006.

11 Q. Tang, G. Zhang, B. Jiang, D. Ji, H. Kong, K. Riehemann, Q. Ji and H. Fuchs, *Smart Mater.*, 2021, **2**, 109–118.

12 W. Yao, Y. L. Yan, L. Xue, C. Zhang, G. P. Li, Q. D. Zheng, Y. S. Zhao, H. Jiang and J. N. Yao, *Angew. Chem., Int. Ed.*, 2013, **52**, 8713–8717.

13 S. K. Park, J. H. Kim, T. Ohto, R. Yamada, A. O. F. Jones, D. R. Whang, I. Cho, S. Oh, S. H. Hong, J. E. Kwon, J. H. Kim, Y. Olivier, R. Fischer, R. Resel, J. Gierschner, H. Tada and S. Y. Park, *Adv. Mater.*, 2017, **29**, 1701346.

14 S. Z. Li and D. P. Yan, *ACS Appl. Mater. Interfaces*, 2018, **10**, 22703–22710.

15 W. G. Zhu, Y. P. Yi, Y. G. Zhen and W. P. Hu, *Small*, 2015, **11**, 2150–2156.

16 J. Zhang, J. H. Tan, Z. Y. Ma, W. Xu, G. Y. Zhao, H. Geng, C. A. Di, W. P. Hu, Z. G. Shuai, K. Singh and D. B. Zhu, *J. Am. Chem. Soc.*, 2013, **135**, 558–561.

17 Y. J. Liu, A. S. Li, S. P. Xu, W. Q. Xu, Y. Liu, W. J. Tian and B. Xu, *Angew. Chem., Int. Ed.*, 2020, **59**, 15098–15103.

18 Y. F. Chen, J. Li and J. B. Gong, *ACS Mater. Lett.*, 2021, **3**, 275–281.

19 D. A. Kunkel, J. Hooper, B. Bradley, L. Schlueter, T. Rasmussen, P. Costa, S. Beniwal, S. Ducharme, E. Zurek and A. Enders, *J. Phys. Chem. Lett.*, 2016, **7**, 435–440.

20 L. J. Sun, W. G. Zhu, W. Wang, F. X. Yang, C. C. Zhang, S. F. Wang, X. T. Zhang, R. J. Li, H. L. Dong and W. P. Hu, *Angew. Chem., Int. Ed.*, 2017, **56**, 7831–7835.

21 Y. Wang, H. Wu, P. H. Li, S. Chen, L. O. Jones, M. A. Mosquera, L. Zhang, K. Cai, H. L. Chen, X. Y. Chen, C. L. Stern, M. R. Wasielewski, M. A. Ratner, G. C. Schatz and J. F. Stoddart, *Nat. Commun.*, 2020, **11**, 4633.

22 R. J. Dillon and C. J. Bardeen, *J. Phys. Chem. A*, 2011, **115**, 1627–1633.

23 Y. Q. Sun, Y. L. Lei, X. H. Sun, S. T. Lee and L. S. Liao, *Chem. Mater.*, 2015, **27**, 1157–1163.

24 Y. L. Lei, Y. Jin, D. Y. Zhou, W. Gu, X. B. Shi, L. S. Liao and S. T. Lee, *Adv. Mater.*, 2012, **24**, 5345–5351.

25 Y. J. Huang, J. Xing, Q. Y. Gong, L. C. Chen, G. F. Liu, C. J. Yao, Z. R. Wang, H. L. Zhang, Z. Chen and Q. C. Zhang, *Nat. Commun.*, 2019, **10**, 9.

26 Y. J. Huang, Q. Y. Gong, J. Ge, P. P. Tang, F. Yu, L. Xiao, Z. R. Wang, H. D. Sun, J. Yu, D. S. Li, Q. H. Xiong and Q. C. Zhang, *ACS Nano*, 2020, **14**, 15962–15972.

27 G. R. Hanson, P. Jensen, J. McMurtrie, L. Rintoul and A. S. Micallef, *Chem. – Eur. J.*, 2009, **15**, 4156–4164.

28 Y. Wang, W. G. Zhu, W. N. Du, X. F. Liu, X. T. Zhang, H. L. Dong and W. P. Hu, *Angew. Chem., Int. Ed.*, 2018, **57**, 3963–3967.

29 W. G. Zhu, L. Y. Zhu, Y. Zou, Y. S. Wu, Y. G. Zhen, H. L. Dong, H. B. Fu, Z. X. Wei, Q. Shi and W. P. Hu, *Adv. Mater.*, 2016, **28**, 5954.

30 D. P. Yan, H. J. Yang, Q. Y. Meng, H. Y. Lin and M. Wei, *Adv. Funct. Mater.*, 2014, **24**, 587–594.

31 H. D. Wu, F. X. Wang, M. Zhang and G. B. Pan, *Nanoscale*, 2015, **7**, 12839–12842.

32 Y. Q. Sun, Y. L. Lei, L. S. Liao and W. P. Hu, *Angew. Chem., Int. Ed.*, 2017, **56**, 10352–10356.

33 C. H. Doi, Z. X. O. Wei, Z. Chen, X. Y. Liu, J. H. Fan, J. F. Zhao, C. Zhang, Z. Y. Pang and S. H. Han, *Adv. Opt. Mater.*, 2019, **7**, 1900838.

34 M. Pawlicki, H. A. Collins, R. G. Denning and H. L. Anderson, *Angew. Chem., Int. Ed.*, 2009, **48**, 3244–3266.

35 R. Li, J. F. Li, Y. J. Sun, X. T. Zhang and W. P. Hu, *ChemPlusChem*, 2019, **84**, 1245–1248.

36 E. D. Lorance, W. H. Kramer and I. R. Gould, *J. Am. Chem. Soc.*, 2002, **124**, 15225–15238.

37 Y. Ito, S. Endo and S. Ohba, *J. Am. Chem. Soc.*, 1997, **119**, 5974–5975.